doi.org/10.36721/PJPS.2021.34.4.SUP.1607-1614.1

Fabrication and characterization of itraconazole loaded anisotropic solid lipid-mannitol microstructures for enhanced antifungal activity

Zunaira Afzal and Sajid Asghar*
Department of Pharmaceutics, Faculty of Pharmaceutical Sciences, Government College University, Faisalabad, Pakistan

Abstract: Anisotropic microparticles containing flower like morphologies have recently attracted significant attention due to their potentially varied application range. Aim of the present work was to build an anisotropic drug delivery system (ASLMMSs) for the encapsulation and enhancement of antifungal activity of a hydrophobic antifungal drug i.e. itraconazole (IRL) with the combination of lipophilic (lipids) as well as hydrophilic (mannitol) materials. Encapsulation efficiency (EE) due to glyceryl monosteatrate (G.ASLMMSs) was 89.02%, whereas Precirol ATO5 formulation (P.ASLMMSs) showed 96.98% EE. FTIR analysis discovered the hydrogen bonding and Vander Waal's forces between lipids and mannitol, while evaluation of XRD data revealed the detailed structural and microstructural characterization indicating the crystallinity of final formulations. Observation under SEM revealed that the final formulations grew in the form of flower like morphologies. These flower-like structures were more obvious for P.ASLMMSs. The increment in dissolution rate (>80% in 6h) could be attributed to the mannitol. Dilutions of Itraconazole loaded anisotropic solid lipid mannitol microstructures (ASLMMSs) in water at concentration range of (500µg/mL, 250µg/mL, 125µg/mL and 75µg/mL) exhibited increased antifungal activity, while free IRL dilution in water showed no zone of inhibition. Both formulations, specifically P.ASLMMSs could signify a promising drug delivery system for lipophilic antifungal drugs.

Keywords: Itraconazole, anisotropic, microparticles, glycerol monostearate, Precirol ATO 5.

INTRODUCTION

Itraconazole (IRL) is a broad spectrum, orally active, classic lipophilic triazole antimycotic agent (log P>5.5) that belongs to BCS class II (Ren *et al.*, 2020). Even though it is effective locally as well as systemically against numerous fungal species, its poor aqueous solubility (~1ng/mL at pH 7.4 and ~4µg/mL at pH 1) retards its absorption from GIT (Ojo *et al.*, 2020). Enhancement in bioavailability of IRL has also been reported when co-administered with food having lipid or fatty contents (Lindsay *et al.*, 2018). Although, BCS II drugs are afflicted by poor solubility, yet their easy penetration through biological membrane and ultimate success at desired site of action via systemic circulation make them a suitable candidate to be loaded in various drug delivery systems (DDS) (Baghel *et al.*, 2016). By enhancing solubility and dissolution rate of these lipophilic compounds, after following various strategies, obviously improves their bioavailability and hence overcoming the main problem of this class. For solubility and dissolution increment, various DDS have been established, containing solid dispersion, solid solution, complexes and solid lipid micro and nanoparticles (Passos *et al.*, 2020).

Lipid based DDS have been the choice of formulation scientists, from last three decades, while constructing delivery system for the BCS class II drugs. Main reasons for choosing lipids over polymeric systems as carrier are their provision of increased encapsulation efficiency for lipophilic drugs being biocompatible and biodegradable, their superior safety profile and ability to slowly release the drug over time thus instituting a doorway towards controlled release of the payload (Pandya *et al.*, 2018). Lipid based systems can be in the form of nanoemulsion, microemulsion, self-emulsifying or self microemulsifying delivery systems (SEDDS/SMEDDS), liposomes, solid lipid nanoparticles (SLNs) and solid lipid microparticle (SLMs). When lipid based system is articulated in the form of SLMs, these cover the lipophilic drug molecules in an efficient way thus improving drug's encapsulation efficiency and stability and hence minimizing drug degradation (Kashkooli *et al.*, 2020). As solid lipids are utilized in the manufacturing of SLMs, that's why SLMs can keep their solid state at room temperature. Their powdered/solid appearances enhance their acceptability for further processing into multiple dosage forms. Furthermore, production of SLMs is usually one-step emulsification process, so, their large-scale manufacturing by utilizing homogenizers, spray dryer and spray congealer is also feasible.

The most frequently used solid lipids for the fabrication of solid lipid microparticle are glyceryl monostearate (GMS), Compritol 888 ATO, Precirol ATO 5, Gelucire 50/13 and stearic acid. We selected GMS and Precirol ATO 5 for loading IRL as they are FDA-approved excipients and commonly used in the production of SLMs and SLNs (Becker *et al.*, 2015). Despite the advantages of

**Corresponding author:* e-mail: sajuhappa@gmail.com; sajidasghar@gcuf.edu.pk

lipids, formulators also encounter various difficulties such as initiation of lipid crystallinity (polymorphic changes) during storage that ultimately leads towards drug expulsion from SLMs. Furthermore, agglomeration and stickiness of lipids can affect product stability (Rathod *et al.*, 2020). Such problems are not stumbled upon by formulators for polymeric systems (Ćetković *et al.*, 2019).

Mannitol (MNT) is an excellent polymeric excipient due to its less hygroscopic nature, capability to reduce the aggregation and cohesiveness in particles, thermal stability, and ability to morph into anisotropic structures (Lin *et al.*, 2017). Furthermore, it has also been reported that MNT improves the release behavior of hydrophobic drugs (Guerreiro *et al.*, 2019). While considering numerous goals such as, enhanced bioavailability of poorly soluble active component plus development of highly stable anisotropic particles appropriate for oral delivery of drug, the combination of both polymer and lipid seems more intriguing. This study reports anisotropic solid lipid-mannitol microstructures (ASLMMSs) for oral administration of IRL. To increase encapsulation of the IRL, it was first encased within SLMs of GMS or Precirol ATO5. These SLMs were then exposed to MNT to be coated as shell. The development of anisotropic microcrystalline structures by MNT was envisaged as the solution to the drug expulsion problem associated with the SLMs and enhancement in dissolution and increment in biological activity of IRL.

MATERIALS AND METHODS

Materials

All reagents and chemicals were purchased from commercial sources and used as received without further treatment. Itraconazole (IRL) was obtained from Nanjing Sen BeiJia Biological Technology Co., Ltd., China. Glyceryl monostearate (GMS), Precirol ATO 5 and Poloxamer 188 (P 188) were purchased from Sigma Aldrich, United States. Mannitol (MNT) was obtained from Saffron Pharmaceuticals, Faisalabad. Dichloromethane (DCM) and Sabouraud Dextrose agar (SDA) were bought from Icon Chemicals, India and Research Product International, USA, respectively.

Preparation of ASLMMs

ASLMMSs loaded with IRL were formulated by emulsification-solvent evaporation technique in conjunction with lyophilization. At room temperature, weighed quantity of IRL and lipid were dissolved in DCM as lipophilic phase for emulsification. For preparation of aqueous phase, 2% aqueous solution of surfactant (P 188) was prepared. Lipophilic phase and aqueous phase were mixed together while homogenizing at 14000 rpm for 2 min (Wu *et al.*, 2018). The formed emulsion was then transferred to magnetic stirrer for removal of DCM. Stirring rate was adjusted at 700 rpm for 6 h at room temperature. Afterwards, water was added in SLMs' suspension for purpose of washing, and centrifugation was carried out at 19000g (Centrifuge 5424R, Eppendorf, Germany). Washing was repeated three times for the complete removal of surfactant and unencapsulated drug. The precipitates obtained after washing/centrifugation were suspended in 10% MNT aqueous solution (Ammar *et al.*, 2016). That suspension was then placed overnight in freezer at -80° C. Frozen material was then lyophilized for 24 h in Christ Alpha 1-2 LD Plus Lyophillizer (Martin Christ Gefriertrocknungsanlagen GmbH, Germany) for formation of ASLMMSs.

Entrapment efficiency (EE) of IRL

EE of ASLMMSs loaded with IRL was determined indirectly by calculating the unencapsulated drug (Wu *et al.*, 2018). Supernatant obtained from washing and centrifugation of the SLMs at 19000g for 15 min was assayed spectrophotometrically (Bachhav *et al.*, 2017) at λmax of 259 nm. EE was calculated using following equation.

$$\text{EE}\,(\%)\frac{\text{W(initial IRL)} - \text{W(free IRL)}}{\text{W(initial IRL)}} \times 100$$

where W (initial IRL) is the weight of drug added to the system, while W (free IRL) is the analyzed weight of IRL in the supernatant.

Characterization of solid lipid microparticles

Fourier transforms infrared spectroscopy (FTIR)

For evaluation of the interaction among IRL, MNT and lipid, attenuated total reflection fourier transformed infrared (ATR-FTIR) spectroscopy was performed with the help of Bruker FTIR spectrometer furnished with A225/Q Platinum ATR multiple crystals CRY diamond. The analysis was conducted in the range of 4000-400cm^{-1}.

X-ray diffraction (XRD)

Powder XRD studies of IRL, lipid, MNT, and IRL loaded ASLMMSs were acquired by using 3805 PANlytical Powder X-Ray Diffractrometer. Scanning of samples of IRL, GMS, Precirol ATO 5, MNT and formulations was performed at a voltage of 45KV and a beam current of 50 mA in the region of $0^{\circ} \leq 2\Theta \geq 70^{\circ}$. The step size was 0.02° and scanning speed was 30 seconds. Cu cathode was used to create X-Rays (Khan *et al.*, 2019).

Scanning electron microscopy (SEM)

For determination of shapes of IRL, MNT, and ASLMMSs, SEM analysis was performed by utilizing JEOL Model JSM-6490 (Tokyo Japan). Samples were placed on double adhesive tape, stuck to an aluminum stub and coated with thin layer of gold under vacuum so as to make them electrically conductive. Photomicrograph of IRL, MNT, and ASLMMSs were achieved at magnification levels of 5000x, 3500x, 2500x, 1500x, 1000x, 650x, 500x and 150x at 10KV. The micron marker

levels of SEM were adjusted at 100µm, 50µm, 20µm, 10µm and 5µm.

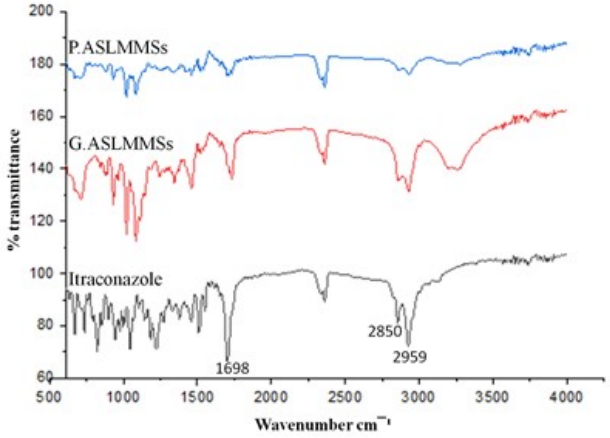

Fig. 1: FTIR spectra of IRL, G.ASLMMSs and P.ASLMMSs.

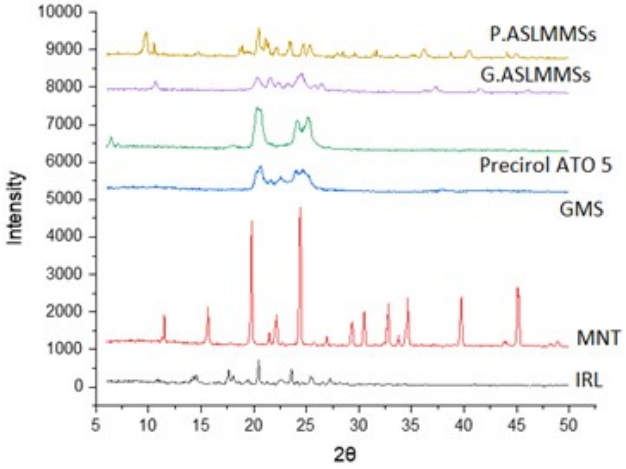

Fig. 2: XRD diffractograms of IRL, MNT, GMS, Precirol ATO5, G.ASLMMs, and P.ASLMMs.

In vitro drug release studies

In vitro drug release study was performed as described elsewhere with slight modifications using cellophane membrane bag that had the molecular weight cutoff 10 kDa (Lin *et al.*, 2017). First of all, dialysis bags were thoroughly washed and then soaked in distilled water overnight. Concisely, weighed amount of powdered ASLMMSs equivalent to 100mg of IRL were added in overnight-soaked cellophane membrane bags, and these bags were sealed with clips on both ends to prevent any leakage. These bags were carefully introduced into dissolution media (900mL of acidic media, pH 1.2) having 0.3% sodium dodecyl sulphate (SDS). SDS was used to maintain sink condition (Patil-Gadhe and Pokharkar, 2014). These experiments were performed in USP type II dissolution apparatus (Pharma Test, Germany) at a paddle rotation speed of 50 rpm and temperature was maintained at 37°C. Five milliliters of samples were withdrawn at a predefined time interval of 5, 10, 15, 30, 45, 60, 90, and 120 min. After completion of 120 min in 1.2 pH buffer, these cellophane membrane bags were shifted to 900 mL of 6.8 pH phosphate buffer dissolution media while maintaining all other experimental conditions. Time interval for fluid withdrawal was adjusted at 150, 180, 240, 300, 360, 420, 480, and 600 min. The dissolution media (pH 1.2 and pH 6.8) were replenished with the fresh dissolution fluid of the same composition after each withdrawal. The amount of IRL was determined by UV spectrophotometer at 259 nm wavelength. Each test was performed in triplicate.

Table 1: EE % of IRL of freshly prepared ASLMMSs and after 3 months storage at room temperature.

Formulations	EE (%)	
	Fresh Formulations	After 3 months Storage
P.ASLMMS	89.02	87.36
G.ASLMMS	96.98	95.15

In vitro antimycotic activity

The *in vitro* antimycotic activity of IRL and ASLMMSs was evaluated by following the previously reported method with slight modifications (Alhowyan *et al.*, 2019). SDA media was prepared as per manufacturer's instructions. 32.5g SDA was dissolved in 500mL distilled water and sterilized using autoclave at 15 psig pressure for 15min at a temperature of 121°C. Afterwards, sterilized SDA was transferred and solidified into petri plates, and suspension of Candida albicans (C. albicans) adjusted at inoculum concentration of 108 CFU/mL in 0.9% NaCl was seeded over the media. Four wells each of 10 mm in diameter were excised from agar of each petri plate and filled with 100µL of four dilutions (500µg/mL, 250µg/ml, 125µg/mL, 75µg/mL) of each formulation. Same dilutions of IRL in DMSO or water were also filled in separate petri dishes. Incubation of plates were done at 35˚C for 48 hrs and zones of inhibition were determined.

Stability studies

To evaluate stability of IRL loaded ASLMMs, formulations were stored at room temperature (30 ± 1°C) for 3 months in stoppered glass vials and assessed for EE as reported in literature (Alhowyan *et al.*, 2019).

STATISTICAL ANALYSIS

Percent and standard deviation were calculated using Microsoft Excel and GraphPad Prism. Statistical comparison of the dissolution profiles was made by F2-similartity index identified through the DDSolver.

RESULTS

Entrapment Efficiency (EE) of itraconazole

The IRL entrapment efficiency in ASLMMSs formulations consisting of GMS and Precirol ATO5 were

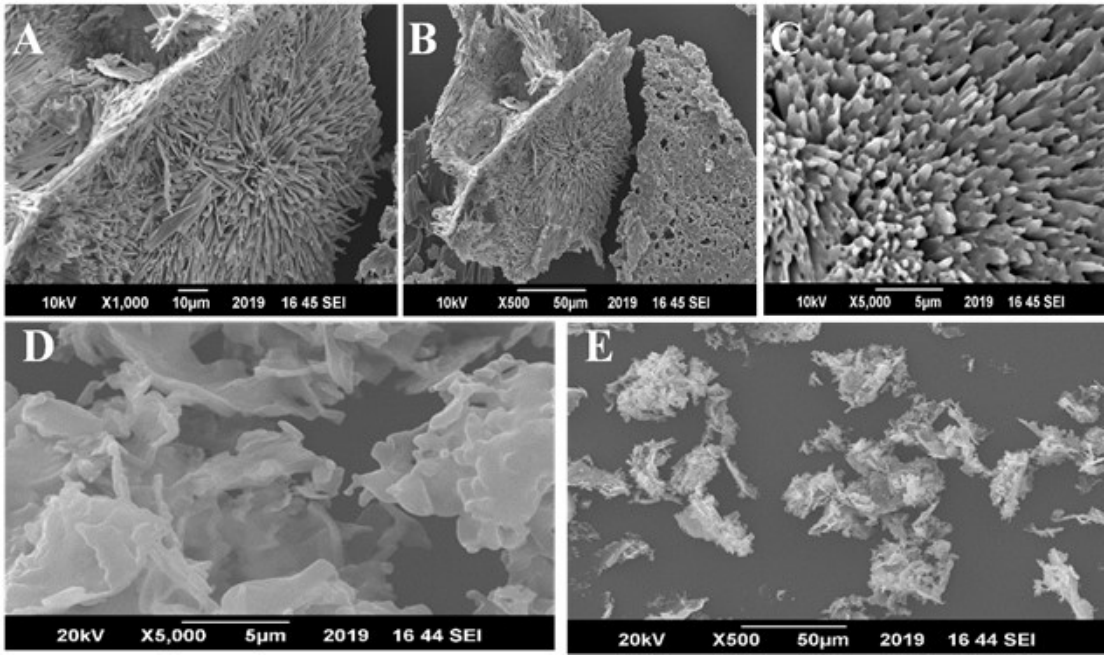

Fig. 3: SEM images of P.ASLMMSs (A, B, C) and G.ASLMMSs (D, E).

quite different. ASLMMSs containing GMS (G.ASLMMSs) showed 89.02% EE and ASLMMSs containing Precirol ATO5 (P.ASLMMSs) showed 96.98 % EE.

Fourier transforms infrared spectroscopy (FTIR)

FTIR was utilized to conclude the intermolecular interactions between lipids and MNT. It also evaluated the encapsulation of IRL in our carrier. When pure IRL's FTIR spectrum was observed, it showed IRL characteristic peak of NH_2 group at 3136 cm^{-1} and C-H band at 2959cm^{-1}. Aliphatic C-H bond showed band stretching at 2850cm^{-1} while C=O bond showed its presence at 1698cm^{-1} as shown in fig. 1. All these bands and peaks were in accordance with the previous reports (Nesseem, 2001). MNT presented its characteristic broad band at 3000 cm^{-1} due to vibration of axial deformation of O-H. The other bands of MNT appeared at 1458 cm^{-1}, 1145 cm^{-1} and 1083 cm^{-1} and were are present in both formulations due to axial vibration of C-O in alcoholic group (Mirza *et al.*, 2016). The characteristic peaks of GMS and Precirol ATO5 from 1700-1750 cm^{-1} corresponding to C=O were observed in the formulations but its intensity decreased in both formulations (Kamble *et al.*, 2010). Second peak that belongs to C-H stretching and was characteristic of stearate appeared at 2931cm^{-1} in both formulations (Kallakunta *et al.*, 2018). The broadening of the peak from 2940-3200cm^{-1} and sharpness of peak at 2930cm^{-1} in both formulations was also observed.

X-ray diffraction (XRD)

XRD pattern is utilized for comprehension of different components by forming diffraction peaks at 2θ range (Thapaliya *et al.*, 2019). The diffractogram (2θ versus % intensity) can be reflected as finger print of material and assists in interpretation of various crystalline structures of the materials and DDS (Mirza *et al.*, 2016). The prospective variations in the crystalline structure of pure IRL, Precirol ATO5, GMS, MNT and ASLMMSs were scrutinized by modification in the intensity of diffraction peaks and shift. These changes are demonstrated in fig. 2. IRL powder posed characteristic peaks at 14.54 θ, 17.6θ, 20.5θ, 23.6 θ, 25.3θ and 27.22θ (Lin *et al.*, 2017, Mirza *et al.*, 2016). Definite peaks of MNT appeared at 10.5θ, 18.8θ, 23.44θ, 25.9θ, 29.45θ, 31.8θ, 33.7θ. 38.8θ, and 44.1θ (Malamatari *et al.*, 2016). Likewise, diffractogram of both lipids were examined individually. GMS exhibited its peaks at 19.67θ, 21.63θ, 21.49θ, 23.73θ and 23.65θ, while Precirol ATO 5 showed peaks at 5.3θ, 19.3θ, 23.16θ and 24.15θ which agree with the previous studies (Agarwal *et al.*, 2020). In both formulations, the characteristic peaks of drug, especially at 14.54θ, 17.6θ, 25.3θ and 27.22θ diminished. Characteristic peaks shift of MNT occurred in the formulations e.g. 10.5θ shifted to 9.745 and 18.8θ shifted to 18.1θ. While the peak of MNT at 23.4θ became sharper and more prominent, whereas, peak at 25.9θ shifted to 25.3θ in both formulations. Presence of peaks at 29.45θ, 31.8θ, 33.7θ. 38.8θ, 44.1θ were attributed towards MNT.

Scanning electron microscope (SEM)

Before addition of MNT and executing the process of freeze drying, optical microscopic analysis was performed. That examination was accomplished to inspect the preparation and morphology of SLMs, which would act as seeds for MNT deposition in next stages. SEM studies revealed the appearance of anisotropic shapes of

ASLMMSs which differed from the spherical particles mentioned in literature. The selection of materials, conditions and method of preparation determine the morphologies of particles (Seedat *et al.*, 2016). The morphology of final formulations varied from sheets having small nano-projections to dandelion like microstructures. These diversified arrangements of MNT over SLMs during freezing/lyophilization steps, depend upon the dissimilar nature of lipids used. G.ASLMMSs showed the arrangement of mannitol in the form of sheets at low magnification of SEM. At high magnification (5000x) of SEM, these sheets exhibited small projections. While, P.ASLMMSs displayed itself under low magnification of 500x as sheets having spikes, but at 1000x, these ASLMMSs appeared as dandelion-flower like structure as shown in fig. 3. At 5000x magnification, spacing between these projections can be observed.

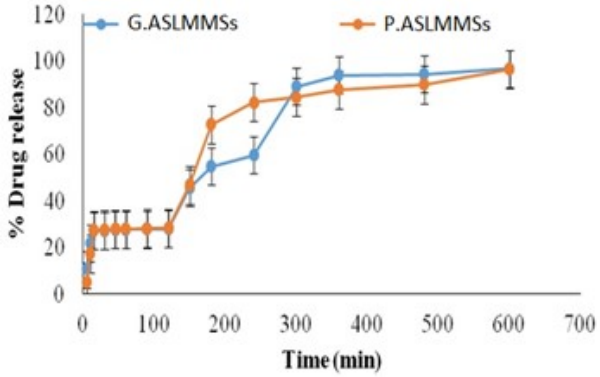

Fig. 4: Release of itraconazole from GMS SLPMSs and Precirol SLPMSs at pH 6.8 phosphate buffer

In vitro drug release studies

The IRL release in 1.2 pH acidic media was about 28 % at the end of 2 h. At 6.8 pH phosphate buffer, drug release reached more than 80 % within 6 h as shown in fig. 4. It showed a biphasic drug release behavior from the ASLMMSs. Comparison of dissolution profiles was made by finding out the similarity index through DDSolver software. It was revealed that dissolution profiles of both formulations were not similar at pH 6.8 phosphate buffer (F2 value= 46.94).

In vitro antimycotic activity

The antifungal activity of IRL loaded ASLMMSs against C. albicans was investigated as shown in fig. 5. The solution of drug was made in dimethyl sulfoxide (DMSO) because drug did not show any inhibition zones when dispersed in water. Complete dissolution of IRL in DMSO resulted in enhanced antifungal activity. Unlike IRL, both formulations were dispersed in water and showed enhanced antifungal activity as compared to previously reported formulation approaches (Mohanty *et al.*, 2015, Qumber *et al.*, 2020). P.ASLMMSs displayed increased antifungal activity as compared to G.ASLMMSs.

Stability studies

The result of stability studies of IRL loaded formulations revealed no obvious changes in entrapped content of both formulations after 3 months of storage at room temperature as shown in table 1.

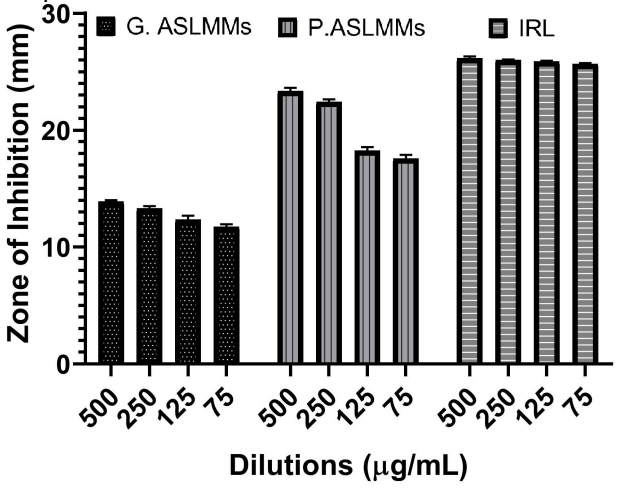

Fig. 5: Zone of inhibition of IRL in DMSO, P.ASLMMSs and G.ASLMMSs in water.

DISCUSSION

In this study, we report a method consisting of solvent evaporation method followed by lyophilization to prepare drug loaded microstructures of versatile shapes for oral administration. For the development of our formulations, lipids were selected because these have different wetting properties as compared to MNT. That characteristic increased the anisotropic ability during particle formation and interesting geometry achieved in both formulations made up of GMS and Precirol ATO 5. Prepared SLMs at the level of emulsification acted as lipophilic seeds for the deposition of MNT monomer over these. Due to different wetting properties of MNT and lipids, MNT began to deposit in crystalline form over SLMs nucleus, ultimately creating various shapes with passage of time (Hou *et al.*, 2019). This phenomenon of MNT growth is based on well-established theory of interparticle growth. This theory demonstrates that monomers or molecules diffuse along the surface of a nanomaterial to change the shape of the particle with time (Thanh *et al.*, 2014).

GMS is a mono ester while Precirol ATO5 is a diester in nature. The drug solubilization or entrapment inside lipids is also influenced by the presence of mono- and diglycerides. The increased EE of P.ASLMMSs as compared to G.ASLMMSs is due to the presence of mixture of mono-, di- and tri-glycerides in different proportions. These esters of different chain lengths in Precirol ATO5 form less ordered crystals with many imperfections in its structure and that characteristic allows more molecules of drugs to get entrapped inside the lipids. (Mirza *et al.*, 2016). Increased lipophilicity of

lipids also contributes towards the increased accommodation of hydrophobic drug. That is evident by comparing HLB values of GMS and Precirol ATO5 i.e. 3.8 and 2, respectively (Vivek *et al.*, 2007).

MNT interaction with lipid plays an important role in the building and formation of our carrier. Interactions that evolved flower like structures mainly employed hydrogen bonding and Vander Waal's forces. In both formulations, the decrease in peak intensities of GMS and Precirol ATO 5 from 1700-1750 cm^{-1} is an indication of involvement of C=O group in hydrogen bonding. (Tatke *et al.*, 2019). Peak broadening of lipids in formulations from 2940-3200 cm^{-1} also hints hydrogen bonding. That hydrogen bonding can be further explained on the basis of appearance of sharp peak at 2930cm^{-1} in both formulations which could be due to hydroxyl stretching (Ma *et al.*, 2019). New broad band appearance at 820cm^{-1} in formulations represents the involvement of Vander Waals forces (De Smet *et al.*, 2014). These intermolecular force lead towards the formation of new structures over particles. The characteristics peaks of IRL got diminished or their intensities got reduced when combined with lipid and MNT. That might be due to total encapsulation of drug inside the particle. No new peak was observed that is endorsing, that no chemical interaction occurred.

Sharp and prominent diffraction peaks of all materials can be detected easily thus signifying their crystalline nature (Thapaliya *et al.*, 2019). Disappearance of the drug's peak at 14.54θ, 17.6θ, 25.3θ and 27.22θ indicated entrapment of drug inside the lipid matrix and MNT structures. The change in intensities of the MNT peaks in formulations may be credited to the changed distribution of crystal orientation in ASLMMSs (Cai *et al.*, 2020). Peak sharpness of lipids was enhanced in diffractrogram of the formulations, due to more ordered crystalline state and development of MNT crystalline architecture. Secondly, by thoroughly examining the diffractrogram of final formulations, new peaks were also grasped. The formation and shifting of peaks give proof of the formation of new morphological structures which were in agreement with the result of FTIR. So, it became obvious that MNT presence enhanced the sharpness and intensity as well as formation of new peaks in diffractrogram thus indicating finally the enhancement of crystallinity of the system.

The diversified shapes of our prepared ASLMMSs might be attributed not only towards different wetting properties of lipid and MNT but also the interaction of MNT with monoester and diesters of selected lipids. The main interaction that leads towards the formation of anisotropic shapes was hydrogen bonding between lipids and MNT that was proved from the FTIR studies. But the difference in anisotropic shapes of both lipids could be approved by the work of Hu *et al* who had proved that by changing the alkyl chain number and position, the final structural morphology of the system could also be changed (Hu *et al.*, 2017). That was also evident from our study that provided architecturally different structures in final formulation, when examined morphologically, even though the concentration of MNT and conditions were same for both lipids. MNT deposition in different ways not only increased the surface area but also provided the shield effect to the lipid containing particles (Mirza and Saha, 2020). Moreover, MNT also act as a cryoprotectant to the whole system while freeze drying process (Mirza *et al.*, 2016).

The abrupt drug release in acidic pH till 28% in both formulations may be due to porous MNT structures that are present in formulation (Saffari *et al.*, 2016). Highly wet table excipients, such as MNT, when interact with dissolution media promote penetration of dissolution media. That increased dissolution media penetration enhanced the release of drug >80% within 6h. MNT microstructures are the main reason of increased release even having the lipid as encapsulating excipients for drug (Lin *et al.*, 2017).

The enhanced antifungal activity against C. albicans may be contributed by the flower like structure of our carrier. These structural morphologies not only increase the surface area of the particles but their geometric tunability increase the interaction of particles with the cell membranes (Mirza and Saha, 2020). These anisotropic particles are taken up by cells more efficiently and rapidly because contact area of these type of particles are high as compared to spherical one. That increased activity of P.ASLMMSs may be attributed towards enhanced EE and increased anisotropic structural morphology when compared with G.SLMMSs. (Jindal, 2017) The long dandelion structure of P.ASLMMSs may be the reason for greater penetration into fungal cells (Ghosh *et al.*, 2020). The biodistribution as well as increased stability of anisotropic shaped particles is also superior as compared to their spherical counterparts (Mirza and Saha, 2020). The utilization of fatty acid ester could also be a reason for enhanced antifungal activity. The activity of fatty acid esters against different fungi especially Candida species has been well established. Hence, higher zones of inhibition against C. albicans might be due to combined activity of IRL and Precirol ATO5 or GMS (Clitherow *et al.*, 2020). Therefore, the use of bioactive lipids for encapsulation of IRL and the construction of flower-like anisotropic microstructures could pave the way for designing oral delivery systems of IRL at lower doses but equivalent antifungal activity.

CONCLUSION

IRL loaded ASLMMSs having flower-like morphologies were successfully formulated using emulsification-solvent

evaporation in conjunction with lyophilization. SEM approved the claim of anisotropic structures. Overall, ASLMMs might be useful system for oral delivery of IRL with much higher encapsulation efficiency, enhanced drug release, and antifungal activity. However, future studies should consider the *in vivo* safety and efficacy in suitable animal models for validating the suitability of ASLMMSs for oral administration in humans.

ACKNOWLEDGEMENT

This work was funded by HEC Pakistan under the grant # 21-1257/SRGP/R&D/HEC/2016.

REFERENCES

Agarwal S, Murthy RSR, Harikumar SL and Garg R (2020). Quality by design approach for development and characterisation of solid lipid nanoparticles of quetiapine fumarate. *Curr. Comput-Aided Drug Des.*, **16**(1): 73-91.

Alhowyan AA, Altamimi MA, Kalam MA, Khan AA, Badran M, Binkhathlan Z, Alkholief M and Alshamsan A (2019). Antifungal efficacy of Itraconazole loaded PLGA-nanoparticles stabilized by vitamin-E TPGS: *In vitro* and *ex vivo* studies. *J. Microbiol. Methods*, **161**: 87-95.

Ammar HO, Ghorab MM, Mahmoud AA and Noshi SH (2016). Formulation of risperidone in floating microparticles to alleviate its extrapyramidal side effects. *Future J. Pharm. Sci.*, **2**(2): 43-59.

Bachhav SS, Dighe VD, Kotak D and Devarajan PV (2017). Rifampicin lipid-polymer hybrid nanoparticles (LIPOMER) for enhanced Peyer's patch uptake. *Int. J. Pharm.*, **532**(1): 612-622.

Baghel S, Cathcart H and O'Reilly NJ (2016). Polymeric amorphous solid dispersions: A review of amorphization, crystallization, stabilization, solid-state characterization, and aqueous solubilization of biopharmaceutical classification system class II drugs. *J. Pharm. Sci.,* **105**(9): 2527-2544.

Becker K, Salar-Behzadi S and Zimmer A (2015). Solvent-free melting techniques for the preparation of lipid-based solid oral formulations. *Pharm. Res.*, **32**(5): 1519-1545.

Cai L, Bian F, Chen H, Guo J, Wang Y and Zhao Y (2020). Anisotropic microparticles from microfluidics. *Chem*., **7**(1): 93-136.

Cetkovic Z, Cvijić S and Vasiljević D (2019). Formulation and characterization of novel lipid-based drug delivery systems containing polymethacrylate polymers as solid carriers for sustained release of simvastatin. *J. Drug Deliv. Sci. Technol.*, **53**: 101222.

Clitherow KH, Binaljadm TM, Hansen J, Spain SG, Hatton PV and Murdoch C (2020). Medium-chain fatty acids released from polymeric electrospun patches inhibit candida albicans growth and reduce the biofilm viability. *ACS Biomater. Sci. Eng.*, **6**(7): 4087-4095.

De Smet L, Saerens L, De Beer T, Carleer R, Adriaensens P, Van Bocxlaer J, Vervaet C and Remon JP (2014). Formulation of itraconazole nanococrystals and evaluation of their bioavailability in dogs. *Eur. J. Pharm. Biopharm.*, **87**(1): 107-113.

Ghosh M, Mandal S, Roy A, Chakrabarty S, Chakrabarti G and Pradhan SK (2020). Enhanced antifungal activity of fluconazole conjugated with Cu-Ag-ZnO nanocomposite. *Mater. Sci. Eng. C*, **106**: 110160.

Guerreiro F, Pontes JF, da Costa AMR and Grenha A (2019). Spray-drying of konjac glucomannan to produce microparticles for an application as antitubercular drug carriers. *Powder Technol.*, **342**: 246-252.

Hou Y, Fang G, Jiang Y, Song H, Zhang Y and Zhao Q (2019). Emulsion lyophilization as a facile pathway to fabricate stretchable polymer foams enabling multishape memory effect and clip application. *ACS Appl. Mater. Interfaces*, **11**(35): 32423-32430.

Hu Y, Miao K, Xu L, Zha B, Miao X and Deng W (2017). Effects of alkyl chain number and position on 2D self-assemblies. *RSC Advances*, **7**(51): 32391-32398.

Jindal AB (2017). The effect of particle shape on cellular interaction and drug delivery applications of micro-and nanoparticles. *Int. J. Pharm.*, **532**(1): 450-465.

Kallakunta VR, Tiwari R, Sarabu S, Bandari S and Repka MA (2018). Effect of formulation and process variables on lipid based sustained release tablets via continuous twin screw granulation: A comparative study. *Eur. J. Pharm. Sci.*, **121**: 126-138.

Kamble R, Kumar A, Mahadik K and Paradkar A (2010). Ibuprofen-glyceryl monostearate (GMS) beads using melt solidification technique: Effect of HLB. *Int. J. Pharm. Pharm. Sci.*, **2**(4): 100-104.

Kashkooli FM, Soltani M and Souri M (2020). Controlled anti-cancer drug release through advanced nano-drug delivery systems: Static and dynamic targeting strategies. *J. Control. Release,* **327**: 316-349.

Khan A, Toufiq AM, Tariq F, Khan Y, Hussain R, Akhtar N and ur Rahman S (2019). Influence of Fe doping on the structural, optical and thermal properties of α-MnO2 nanowires. *Mater. Res. Express*, **6**(6): 065043.

Lin L, Quan G, Peng T, Huang Z, Singh V, Lu M and Wu C (2017). Development of fine solid-crystal suspension with enhanced solubility, stability and aerosolization performance for dry powder inhalation. *Int. J. Pharm.*, **533**(1): 84-92.

Lindsay J, Mudge S and Thompson III GR (2018). Effects of food and omeprazole on a novel formulation of super bioavailability itraconazole in healthy subjects. *Antimicrob. Agents Chemother.*, **62**(12): e01723-01718.

Ma G, Sun J, Zhang Y, Jing Y and Jia Y (2019). A novel low-temperature phase change material based on stearic acid and hexanamide eutectic mixture for

thermal energy storage. *Chem. Phys. Lett.*, **714**: 166-171.

Malamatari M, Somavarapu S, Kachrimanis K, Bloxham M, Taylor KM and Buckton G (2016). Preparation of theophylline inhalable microcomposite particles by wet milling and spray drying: The influence of mannitol as a co-milling agent. *Int. J. Pharm.*, **514**(1): 200-211.

Mirza I and Saha S (2020). Biocompatible Anisotropic Polymeric Particles: Synthesis, Characterization, and Biomedical Applications. *ACS Appl. Bio Mater.*, **3**(12): 8241-8270.

Mirza MA, Panda AK, Asif S, Verma D, Talegaonkar S, Manzoor N, Khan A, Ahmed FJ, Dudeja M and Iqbal Z (2016). A vaginal drug delivery model. *Drug Deliv.*, **23**(8): 3123-3134.

Mohanty B, Majumdar DK, Mishra SK, Panda AK and Patnaik S (2015). Development and characterization of itraconazole-loaded solid lipid nanoparticles for ocular delivery. *Pharm. Dev. Technol.*, **20**(4): 458-464.

Nesseem DI (2001). Formulation and evaluation of itraconazole via liquid crystal for topical delivery system. *J. Pharm. Biomed. Anal.*, **26**(3): 387-399.

Ojo AT, Ma C and Lee PI (2020). Elucidating the effect of crystallization on drug release from amorphous solid dispersions in soluble and insoluble carriers. *Int. J. Pharm.*, **591**: 120005.

Pandya NT, Jani P, Vanza J and Tandel H (2018). Solid lipid nanoparticles as an efficient drug delivery system of olmesartan medoxomil for the treatment of hypertension. *Colloids Surf. B Biointerfaces*, **165**: 37-44.

Passos JS, de Martino LC, Dartora VFC, de Araujo GL, Ishida K and Lopes LB (2020). Development, skin targeting and antifungal efficacy of topical lipid nanoparticles containing itraconazole. *Eur. J. Pharm. Sci.*, **149**: 105296.

Patil-Gadhe A and Pokharkar V (2014). Montelukast-loaded nanostructured lipid carriers: Part I oral bioavailability improvement. *Eur.J. Pharm. Biopharm.*, **88**(1): 160-168.

Qumber M, Alruwaili NK, Bukhari SNA, Alharbi KS, Imam SS, Afzal M, Alsuwayt B, Mujtaba A and Ali A (2020). BBD-based development of itraconazole loaded nanostructured lipid carrier for topical delivery: *in vitro* evaluation and antimicrobial assessment. *J. Pharm. Innov.*, 1-14.

Rathod VR, Shah DA and Dave RH (2020). Systematic implementation of quality-by-design (QbD) to develop NSAID-loaded nanostructured lipid carriers for ocular application: preformulation screening studies and statistical hybrid-design for optimization of variables. *Drug Dev. Ind. Pharm.*, **46**(3): 443-455.

Ren X, Cheng S, Liang Y, Yu X, Sheng J, Wan Y, Li Y, Wan J, Luo Z and Yang X (2020). Mesoporous silica nanospheres as nanocarriers for poorly soluble drug itraconazole with high loading capacity and enhanced bioavailability. *Microporous Mesoporous Mater.*, **305**: 110389.

Saffari M, Ebrahimi A and Langrish T (2016). Nano-confinement of acetaminophen into porous mannitol through adsorption method. *Microporous Mesoporous Mater.*, **227**: 95-103.

Seedat N, Kalhapure RS, Mocktar C, Vepuri S, Jadhav M, Soliman M and Govender T (2016). Co-encapsulation of multi-lipids and polymers enhances the performance of vancomycin in lipid-polymer hybrid nanoparticles: In vitro and in silico studies. *Mater. Sci. Eng C*, **61**: 616-630.

Tatke A, Dudhipala N, Janga KY, Balguri SP, Avula B, Jablonski MM and Majumdar S (2019). *In situ* gel of triamcinolone acetonide-loaded solid lipid nano-particles for improved topical ocular delivery: Tear kinetics and ocular disposition studies. *Nanomaterials*, **9**(1): 33.

Thanh NT, Maclean N and Mahiddine S (2014). Mechanisms of nucleation and growth of nanoparticles in solution. *Chem. Rev.*, **114**(15): 7610-7630.

Thapaliya R, Shrestha K, Sharma A, Dhakal N, Manandhar P, Shrestha S and Bhattarai R (2019). Physicochemical characterization of naproxen microcrystals for colon specific pulsatile drug delivery designed using pulsincap technique. *J. Pharm. Investig.*, **49**(5): 553-564.

Vivek K, Reddy H and Murthy RS (2007). Investigations of the effect of the lipid matrix on drug entrapment, in vitro release, and physical stability of olanzapine-loaded solid lipid nanoparticles. *AAPS Pharm. Sci. Tech.*, **8**(4): 16-24.

Wu C, Baldursdottir S, Yang M and Mu H (2018). Lipid and PLGA hybrid microparticles as carriers for protein delivery. *J. Drug Deliv. Sci. Technol.*, **43**: 65-72.